A statistical study of the response of the dayside equatorial F_2 layer to the main phase of intense geomagnetic storms as an indicator of penetration electric field

N. Balan,[1,2] M. Yamamoto,[2] V. Sreeja,[3] I. S. Batista,[4] K. J. W. Lynn,[5] M. A. Abdu,[4] S. Ravindran,[3] T. Kikuchi,[6] Y. Otsuka,[6] K. Shokawa,[6] and S. Alex[7]

Received 9 August 2010; revised 7 January 2011; accepted 13 January 2011; published 24 March 2011.

[1] The response of the dayside equatorial F_2 layer to the main phases of the 22 intense geomagnetic storms ($Dst < -150$ nT) in 1998–2008 is investigated using the digital ionosonde data from the equatorial stations in Brazilian, Indian, and Australian longitudes together with equatorial electrojet strength and IMF B_z; the storms include 15 superstorms ($Dst < -200$ nT). The observations show that there is a period during all MPs when the F_2 layer peak rises (and falls) rapidly with large peak electron density (Nmax) reduction, the rise velocity strongly correlates with the intensity (Dst) of the storms, and the duration of the Nmax reduction corresponds to that of strong eastward electrojet when IMF B_z remains highly negative. The observations indicate the occurrence of strong eastward prompt penetration electric fields (PPEF) during the rapid F_2 layer response. The PPEF drives the F_2 layer peak rapidly upward, which reduces Nmax due to vertical expansion and diffusion. The results therefore suggest that the rapid F_2 layer response (rapid rise (and fall) of peak height (hmax) with large Nmax reduction) observed by ionosondes can be used to detect the occurrence of the daytime eastward PPEF during intense geomagnetic storms irrespective of season and level of solar activity. The data also show two rare events of strong daytime westward electric fields due to disturbance dynamo and/or prompt penetration. The results are important when radars are not available to monitor the occurrence of the PPEF.

Citation: Balan, N., et al. (2011), A statistical study of the response of the dayside equatorial F_2 layer to the main phase of intense geomagnetic storms as an indicator of penetration electric field, *J. Geophys. Res.*, *116*, A03323, doi:10.1029/2010JA016001.

1. Introduction

[2] The equatorial ionosphere has been known as the root of the several special features observed in the low-latitude (and midlatitude) ionosphere under magnetically quiet and active conditions; review articles have been presented by several scientists [*Anderson*, 1981; *Sastri*, 1990; *Abdu*, 1997; *Rishbeth*, 2000, and references therein]. The special features originate basically from the horizontal orientation of the geomagnetic field over the equator. The northward horizontal magnetic field combined with the eastward horizontal electric field generates the equatorial plasma fountain [*Hanson and Moffett*, 1966] that leads to the special features.

[3] The plasma fountain, which is confined to low latitudes under magnetically quiet conditions [*Balan and Bailey*, 1995], becomes a superfountain [*Balan et al.*, 2009] during the daytime main phase (MP) of intense geomagnetic storms due to prompt penetration electric field (PPEF) [*Kelley et al.*, 2004]. The superfountain in the presence of an equatorward neutral wind causes dramatic increases in the peak electron density (Nmax) and total electron content (TEC) (or positive ionospheric storms) observed at low latitudes and midlatitudes [e.g., *Lin et al.*, 2005; *Maruyama and Nakamura*, 2007; *Vijaya Lekshmi et al.*, 2007; *Lu et al.*, 2008; *Balan et al.*, 2010, and references therein].Around the equator, the region of our interest, the super plasma fountain results in a rapid rise of the ionospheric peak (hmax for real and h_pF_2 for virtual, defined below) with a reduction in peak electron density (Nmax) [e.g., *Balan et al.*, 2009].

[4] Observations of the response of the equatorial ionosphere to the intense geomagnetic storms have been reported by several investigators [e.g., *Batista et al.*, 1991; *Sastri et al.*,

[1]Control and Systems Engineering, University of Sheffield, Sheffield, UK.
[2]RISH, Kyoto University, Kyoto, Japan.
[3]Space Physics Laboratory, Vikram Sarabhai Space Centre, Trivandrum, India.
[4]INPE, Sao Jose dos Campos, Brazil.
[5]Ionospheric Systems Research, Noosaville, Queensland, Australia.
[6]STE-Lab, Nagoya University, Nagoya, Japan.
[7]Indian Institute of Geomagnetism, Navi Mumbai, India.

0148-0227/11/2010JA016001

2000; *Paznukhov et al.*, 2007; *Fejer et al.*, 2007; *Jin and Maruyama*, 2008; *Abdu et al.*, 2008; *Sreeja et al.*, 2009, and references therein]. (For a review see work by *Abdu* [1997].) A common observation stressed in these reports is a rapid F_2 layer rise during the daytime MP of the storms, which is attributed to the eastward PPEF. These observations give the indication that the response of the equatorial F_2 layer to the daytime MP of intense geomagnetic storms can be used as an indicator of eastward PPEF. However, the earlier studies are mainly for single storms, and detailed studies are needed to verify the indication.

[5] In the present paper, we report a statistical study of the response of the dayside equatorial F_2 layer (peak) to the main phase (MP) of the intense storms in 1998–2008. By analyzing the digital ionosonde data from three longitudes during the 22 intense storms ($Dst < -150$ nT) in 1998–2008, the paper shows that a rapid rise (and fall) of the F_2 layer peak with a large Nmax reduction is a common feature during the daytime MP of all superstorms ($Dst < -200$ nT). This feature observed over the equator by ionosondes can therefore be used to detect the occurrence of eastward PPEF. Sections 2–4 describe the data, observations and physical mechanism. Models to support the observations are not included here because such models have been presented earlier [e.g., *Balan et al.*, 2009].

[6] The eastward PPEF originates in the magnetosphere during the passage of CMEs (coronal mass ejections). During the main phase of the storm when IMF B_z is southward, a dawn-to-dusk electric field develops in the magnetosphere. This electric field is communicated along the geomagnetic field lines to the high-latitude ionosphere by region 1 field-aligned currents (R1 FAC), and promptly penetrates to low latitudes with eastward polarity in the dayside and westward polarity in the nightside [e.g., *Kikuchi et al.*, 1978; *Kelley et al.*, 2003]. Although a shielding electric field due to region 2 field-aligned currents (R2 FAC) also grows simultaneously, the electric field due to the R1 FAC remains dominant during the southward IMF B_z. A disturbance dynamo electric field, with westward polarity in the dayside and eastward polarity in the nightside, also develops a few hours after the onset of the geomagnetic storms [e.g., *Blanc and Richmond*, 1980; *Abdu et al.*, 2006]. Therefore, the occurrence of strong daytime eastward and westward electric fields during the main phase of intense storms could be due to prompt penetration and disturbance dynamo, respectively; the westward electric field can also have contributions from R2 FAC.

2. Data

[7] The ionosonde data from the equatorial stations in Brazilian (Sao Luis; 2.6°S, 44.2°W; 1.7°S geomagnetic), Indian (Trivandrum; 8.5°N, 77°E; 0.5°N geomagnetic) and Australian (Vanimo; 12.6°S, 141.4°E; 11.8°S geomagnetic) longitudes during the intense geomagnetic storms ($Dst < -150$ nT) that occurred in 1998–2008 are analyzed; the storms with $Dst > -150$ nT are not considered because they are found to have weak response. Though 31 intense storms ($Dst < -150$ nT) occurred in 1998–2008 only 26 storms are considered, the remaining 5 storms are preceded by another storm. Table 1 lists the number of daytime MP, rapid F_2layer response, normal (or slow) F_2 layer response and storms with no ionosonde data in the three longitudes. Of the 26 storms (listed in section 4), 22 storms including 15 superstorms ($Dst < -200$ nT) have ionosonde data in one of the three longitudes.

Table 1. Daytime Main Phase (MP) and Ionosonde Data[a]

Longitude	Daytime MP	Rapid F_2	Normal F_2	No Data
Brazilian	10	6	2	2
Indian	10	8	0	2
Australian	6	6	0	0
Total	26	20	2	4

[a]List of number of daytime MP, rapid F_2 layer response, normal (or slow) F_2 layer response, and storms with no ionosonde data in three longitudes.

[8] The storm time equatorial electrojet index EEJ(storm) is used as a measure of the equatorial east-west electric fields [e.g., *Alex et al.*, 1986]. The electrojet index is obtained from the horizontal component (H component) of the geomagnetic field at an equatorial station and a low-latitude station in nearly same longitudes. First, the ΔH during the storm period at each station is obtained by subtracting the quiet nighttime minimum value of the H component at each station from the respective storm time values. Then the difference between the ΔH at the two stations gives EEJ(storm). Assuming that the variation of ΔH at low latitudes is due to magnetospheric ring current, the EEJ(storm) represents the storm induced variation of the electric fields in the electrojet.

[9] The 1 min resolution magnetic field data are used to calculate the electrojet index EEJ(storm); 1 h resolution data are used when 1 min resolution data are not available. The magnetic field data at Yap (0.30° dip latitude) and Okinawa (26.75°N magnetic latitude) are used for Australian longitude, and at Thirunelveli (0.67°N magnetic latitude) and Alibag (10.17°N magnetic latitude) are used for Indian longitude; magnetic field data in the same equatorial and off equatorial locations are not available for Brazilian longitude. The IMF B_z data measured by the ACE spacecraft is used for the direction of IMF B_z. *Dst* index is used for the phase of the magnetic storms.

3. Physical Mechanism

[10] The daytime eastward PPEF strengthens the upward $\mathbf{E} \times \mathbf{B}$ drift much above the normal daytime drift. The large upward drift drives the F_2 layer (peak) rapidly upward. As the F_2 layer drifts rapidly upward its (peak) density decreases due to vertical expansion and diffusion of plasma along the field lines. The ionization produced at lower heights is also rapidly drifted upward under the strong electric field though the drift becomes more rapid at higher heights (section 4). In short, the F_2 layer (peak) rises rapidly during an eastward PPEF event with a large reduction in peak electron density (Nmax). If the PPEF continues, the peak height may undergo an unusual (rapid) decrease if the virtual height of the original F_2 peak rises (and expands) above the top range of the ionosonde and when a new F_2 peak developed at lower heights becomes stronger than the original F_2 peak; however, Nmax will continue to decrease (and may remain steady after reaching a minimum value) throughout the duration of the PPEF. Therefore the duration of the large Nmax reduction can be taken as an approximate indicator of the duration of the PPEF. The mechanism of the rapid F_2 layer rise is similar

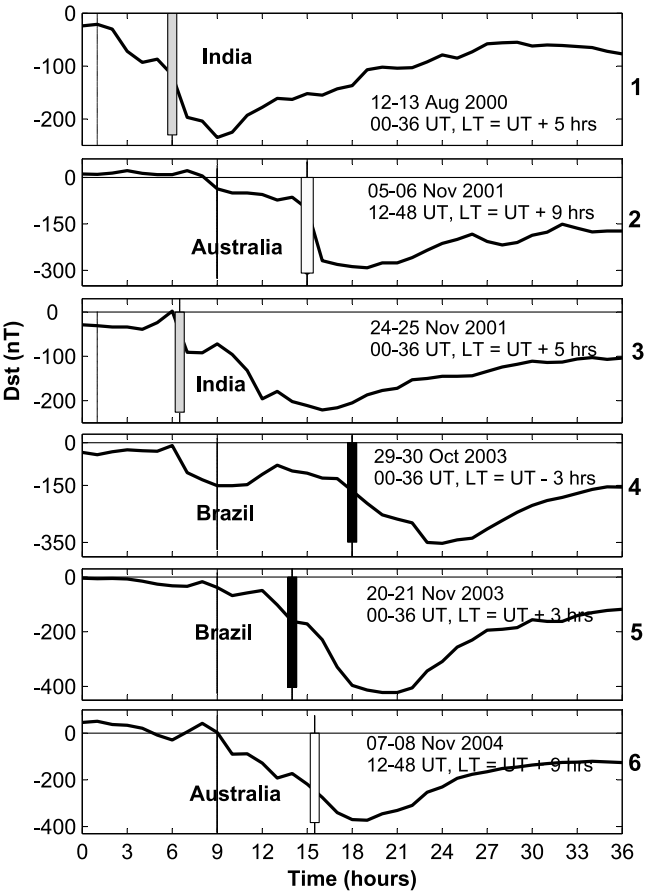

Figure 1. Six geomagnetic storms for which examples of rapid F_2 layer response in three longitudes will be presented (see text).

to the quiet time F_3 layer mechanism [*Balan et al.*, 1998; *Batista et al.*, 2002], but under the strong PPEF the rise becomes so rapid that the usual F_2 layer and F_3 layer separation may not be always observed. For this reason, the signatures of the F_3 layers observed during the rapid F_2 layer rise are not considered in this study.

[11] A rise of the F_2 peak with an average (virtual) velocity of over 30 m s^{-1} is defined as a *rapid rise*, which considers the day-to-day variability of the upward drift under quiet conditions [e.g., *Namboothiri et al.*, 1989; *Fejer et al.*, 1991]. A Nmax (f_oF_2) reduction larger than 2.5 MHz is defined as a *large reduction*; 2.5 MHz is the upper limit of the reduction under quiet conditions [*Lynn et al.*, 2000].

4. Observations

[12] Here we will present two examples each of the rapid F_2 layer response in all three longitudes. Figure 1 shows the six storms for which examples will be presented. The horizontal (time) axis gives the duration of the data (36 h for all storms), with the corresponding UT (and LT) time durations noted in the inset, separately for each storm. The vertical lines represent the times of local sunrise (0600 LT) and vertical bars (with different shades for different longitudes) correspond to the phase of the storms when the rapid F_2 layer response occurred. As shown (Figure 1), all the rapid F_2 layer responses occurred during the daytime MP of the storms.

[13] In the examples, several ionograms will be superposed in Figures 2a, 3a, 4a, 5a, 6a, and 7a to illustrate the rapid uplift of the F_2 layer peak; the ionograms at selected times only are superposed to avoid overcrowding and crossover. The examples also include the true height electron density profiles at selected times (Figures 2b, 3b, 4b, 5b, 6b, and 7b) obtained using the ionosonde software POLAN [*Titheridge*, 1985] and SAO [*Huang and Reinisch*, 1996]. Also included (Figures 2c, 3c, 4c, and 6c) are the

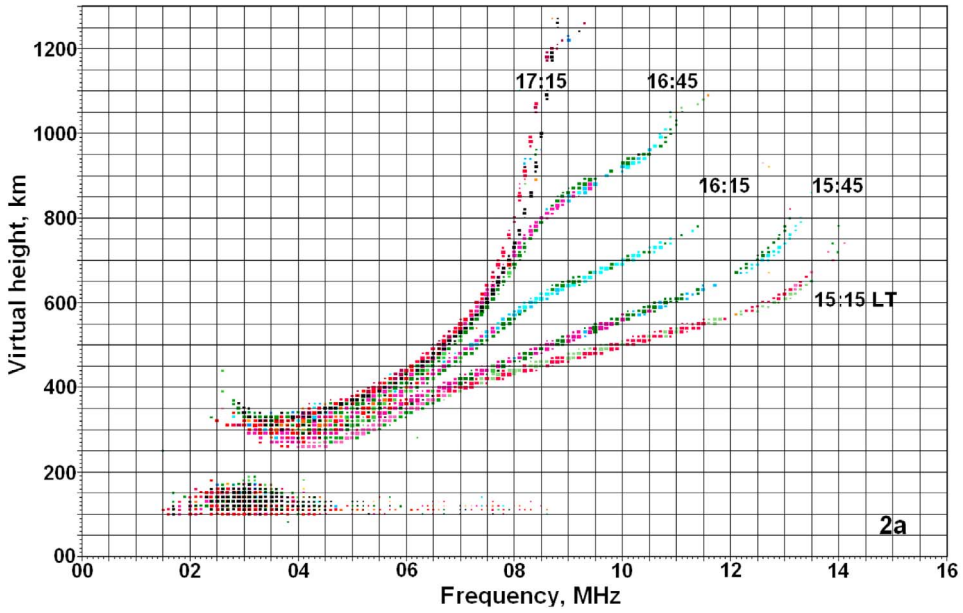

Figure 2a. Five ionograms recorded at the Brazilian equatorial station Sao Luis (2.6°S, 44.2°W; 1.7°S) at selected times during the superstorm of 29 October 2003 (*Dst* = −353 nT) are superposed.

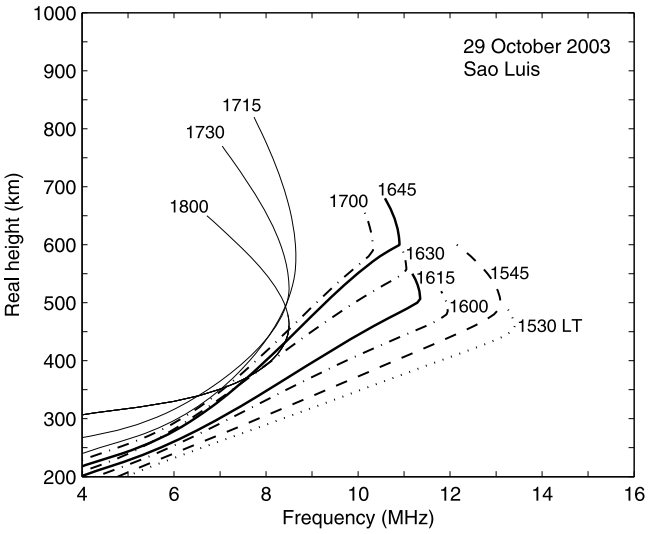

Figure 2b. True height profiles at Sao Luis at selected local times on 29 October 2003.

storm time variations of the F_2 layer peak height h_mF_2 obtained using the software Digion and SAO [*Huang and Reinisch*, 1996] and Nmax (= $1.24 \times 10^4 \times (f_oF_2)^2$ cm^{-3} with f_oF_2 in MHz); these are compared with their variations during 3 quiet days prior to the storms (Figures 2c, 3c, 4c, and 6c) to illustrate the rapid response of the F_2 layer peak during daytime MPs. The variations are also compared with IMF B_z and EEJ(storm) to show that the rapid F_2 layer response corresponds to an eastward PPEF event. For the statistics (section 4.4), the virtual height (h_pF_2) is obtained as h_pF_2 equals the height in the ionogram trace at the frequency equal to $0.834 \times f_oF_2$.

[14] The time variations of h_mF_2 (and h_pF_2) and Nmax are used for the start and end of the rapid response. The start corresponds to the time when h_mF_2 (and h_pF_2) increases faster than normal and Nmax decreases; there can be an uncertainty of up to 15 min between the two. The end corresponds to the time when the steady decrease of Nmax ceases, which can have some uncertainty for the events extending to evening hours when Nmax normally decreases. During the period of the rapid response determined from the steady decrease of Nmax, the peak height in majority of the cases undergoes unusual decreases (following the rapid rise, section 3), and the high-frequency end of the ionogram trace then looks more vertical. Therefore, the real height (hmax) rise and average real rise velocity are calculated from the true height profiles for a period of nearly even rapid hmax rise before h_mF_2 undergoes the first unusual decrease. The average virtual velocity (from h_pF_2) is also calculated for a period before the first h_mF_2 decrease. The duration considered for the real velocity is shorter than that for the virtual velocity in some cases because the real rise is found to be more uneven than the virtual rise.

4.1. Brazilian Longitude

[15] Two examples of the rapid F_2 layer response during the daytime MP of two widely studied superstorms are presented. Figures 2a–2c illustrate the rapid response at Sao Luis (2.6°S, 44.2°W; 1.7°S) during the superstorm of 29 October 2003 (Dst = −353 nT). Five ionograms at selected times are superposed in Figure 2a and true height profiles at selected times are shown in Figure 2b. Figure 2c compares the h_mF_2 and Nmax (first and second panels) during 1200–2400 LT on the superstorm day (thick curves) with those on 3 previous quiet days. As shown by Figures 2a and 2c, until about 1515 LT the ionosphere was behaving normally with h_mF_2 about 460 km and f_oF_2 about 14 MHz. Then f_oF_2 steadily decreases to about 7 MHz by 1900 LT (Figure 2c) giving a rapid response duration of about 3.75 h with a large Nmax (f_oF_2) reduction of about 7 MHz. Within the rapid response period (of Nmax), h_mF_2 rapidly rises to about 620 km, then falls and again rises as discussed in section 3, which continues even beyond 2400 LT; Nmax also continues to decrease. However, the duration of the rapid response is limited to the steady decrease portion of Nmax (and within daytime).

[16] As shown by the true height profiles (Figure 2b), the real rise of hmax is also uneven, and is nearly steady during 1615–1645 LT when hmax rises by about 110 km with an average rise velocity of about 61 m s^{-1}. The virtual height

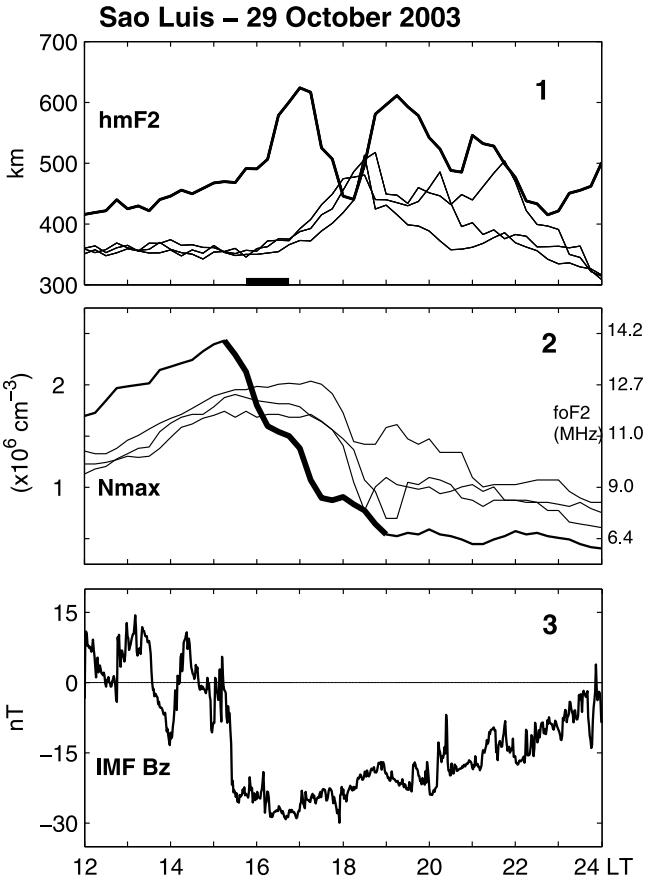

Figure 2c. Variations of h_mF_2 and Nmax (first and second panels) at Sao Luis during 1200–2400 LT on the geomagnetic storm day (29 October 2003, thick curves) compared with those on 3 previous quiet days (thin curves). The small horizontal bar in the first panel represents the duration used for obtaining the virtual rise velocity. The third panel shows the IMF B_z variation on the stormday (shifted by 30 min).

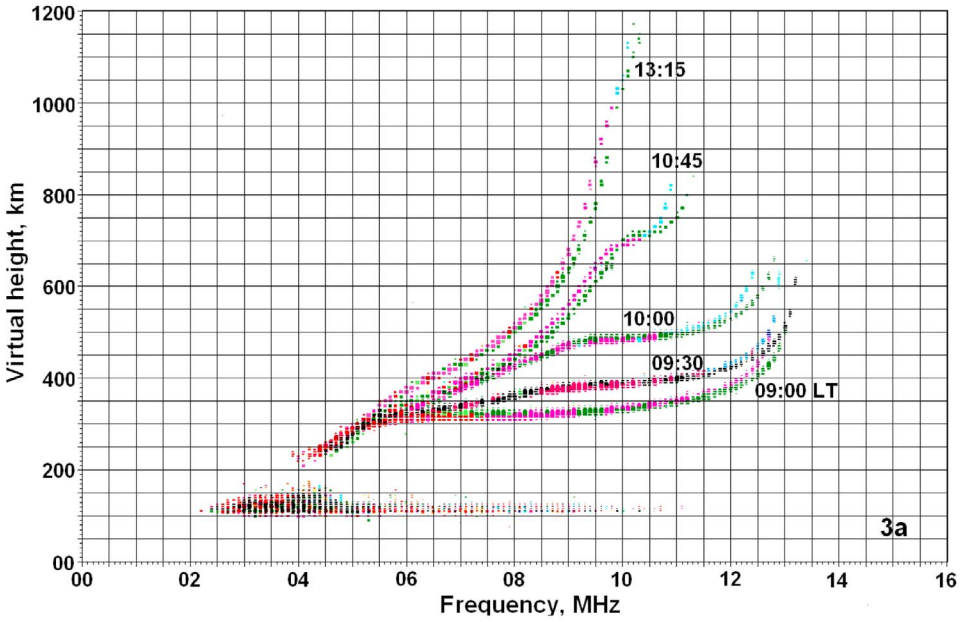

Figure 3a. Five ionograms recorded at the Brazilian equatorial station Sao Luis (2.6°S, 44.2°W; 1.7°S) at selected times during the superstorm of 20 November 2003 (Dst = −422 nT) are superposed.

h_pF_2 (from Figure 2a) is found to rise almost steadily by about 290 km during 1545–1645 LT giving an average virtual rise velocity of about 81 m s^{-1}. As shown by the data in the third panel (Figure 2c), the start of the rapid response corresponds to the time when IMF B_z turned from positive to highly negative (up to −25 nT) during the main phase of the superstorm (Figure 1), which might have caused a large eastward PPEF. However, the end of the rapid response (at 1900 LT) may or may not correspond to the end of the PPEF in this case. Although the rapid vertical rise (and fall) of the F_2 layer peak, with large Nmax reduction, over the equator is a direct indicator of the presence of a strong eastward electric field, a more direct indication of the intensity of the electric field and its duration cannot be provided since no magnetic field data are available to calculate the EEJ strength for this case. In addition to the eastward PPEF, the normal prereversal enhancement of the electric field might have also contributed to the total electric field in this case.

[17] Figures 3a–3c show the rapid F_2 layer response observed over Sao Luis during the superstorm of 20 November 2003 (Dst < −422 nT). Unlike the first example (Figures 2a–2c), which was for afternoon-evening hours, the second example is for morning-afternoon hours. As shown by Figures 3a and 3c, the ionosphere was behaving normally until about 0915 LT when h_mF_2 was about 300 km and f_oF_2 was about 13.5 MHz. Then, f_oF_2 decreases to about 6.5 MHz by 1515 LT giving a rapid response duration of about 6 h and a large f_oF_2 reduction of about 7 MHz; during this period h_mF_2 undergoes fluctuations with a peak value of about 580 km; there is also a period of about 2 h within the duration of the rapid response when f_oF_2 remains steady. As shown by the true height profiles (Figure 3b), hmax rises fastest during 0945–1030 LT by about 110 km with an average rise velocity of about 41 m s^{-1}. The virtual height h_pF_2 (from Figure 3a) rises steadily by about 140 km during 1000–1045 LT giving an average virtual velocity of 52 m s^{-1}. This event happened when IMF B_z was highly negative (up to −50 nT, third panel) during the main phase of the storm (Figure 3c) when an eastward PPEF might have occurred. However, no electric field and magnetic field data are available. The two examples in the Brazilian longitude (Figures 2 and 3) demonstrated that the F_2 layer peak height undergoes rapid rise (and fall) with large Nmax reduction during the daytime MP of superstorms due to eastward PPEF.

4.2. Indian Longitude

[18] The ionograms at selected times superposed in Figure 4a, true height profiles in Figure 4b, and comparison

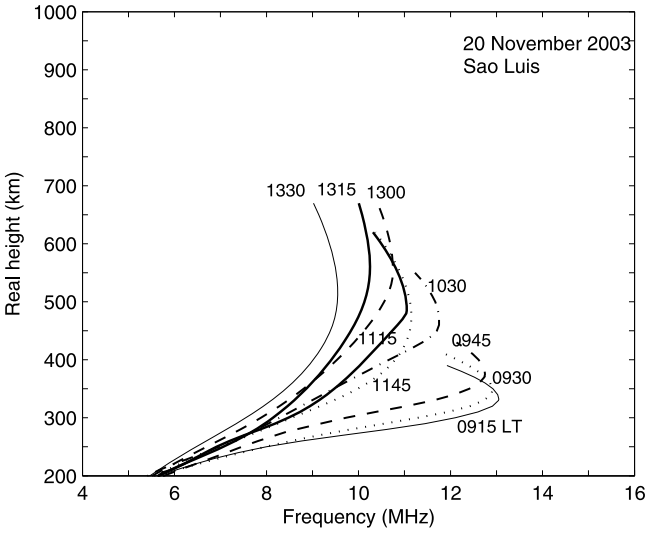

Figure 3b. True height profiles at Sao Luis at selected local times on 20 November 2003.

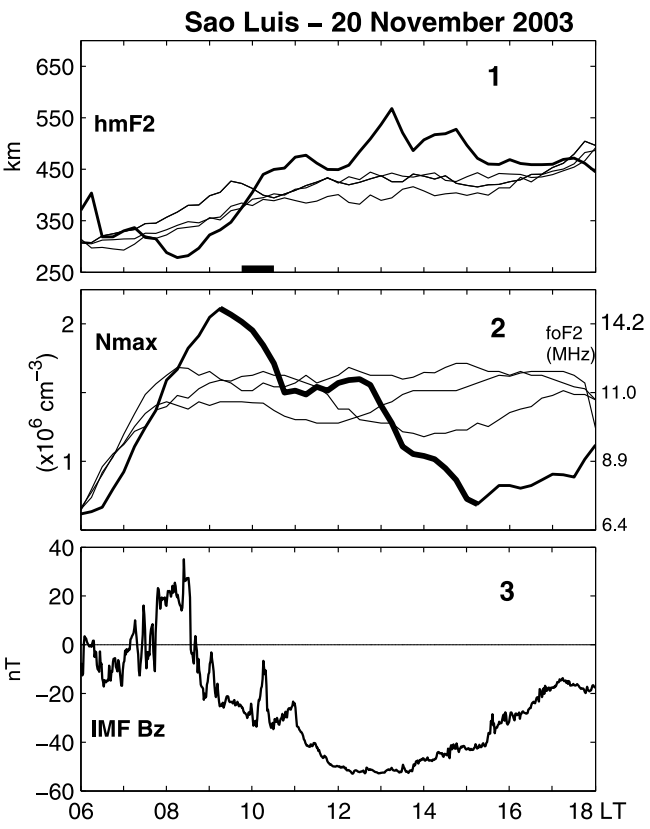

Figure 3c. Variations of h_mF_2 and Nmax (first and second panels) at Sao Luis during 0600–1800 LT on the geomagnetic storm day (20 November 2003, thick curves) compared with those on 3 previous quiet days (thin curves). The small horizontal bar in the first panel represents the duration used for obtaining the virtual rise velocity. The third panel shows the IMF B_z variation on the stormday (shifted by 40 min).

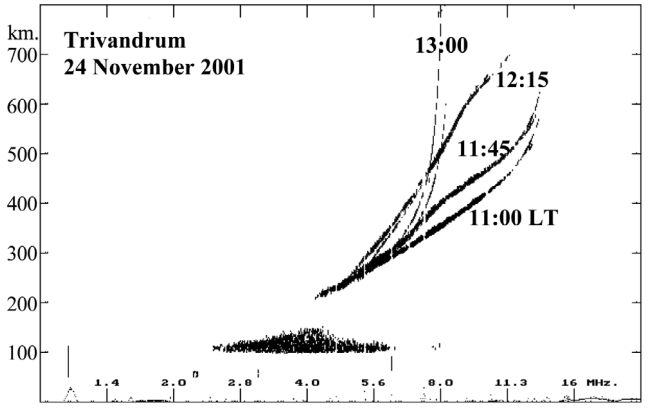

Figure 4a. Four ionograms recorded at the Indian equatorial station Trivandrum (8.5°N, 77°E; 0.5°N) at selected times during the superstorm of 24 November 2001 (Dst = −221 nT) are superposed.

of the storm time variations h_mF_2 and Nmax with their quiet time variations in Figure 4c illustrate the rapid F_2 layer response over the Indian station Trivandrum (8.5°N, 77°E; 0.5°N) during the main phase of the superstorm (Dst = −221 nT) of 24 November 2001. As shown by Figure 4c, Nmax (f_oF_2) undergoes a steady decrease from about 13.5 MHz to 7 MHz during 1130–1245 LT; this gives a short rapid response duration of about 1.25 h and a large f_oF_2 reduction of about 6.5 MHz. After the large decrease around noon Nmax returns to its normal level. Within the rapid response period, h_mF_2 undergoes a rapid rise to about 610 km and a rapid fall (section 3). The true height profiles (Figure 4b) give a real height (hmax) rise of about 130 km during 1145–1230 LT with an average real rise velocity of about 48 m s^{-1}. It may be noted that the true height profiles over Trivandrum does not have the topside electron densities obtained from extrapolations as was done for the Sao Luis (and Vanimo) data. During 1145–1230 LT, the virtual height (h_pF_2) is found to rise by about 150 km, from about 520 km to 670 km, giving a virtual rise velocity of about 56 m s^{-1}. The rapid response started when IMF B_z turned highly negative (up to −30 nT; Figure 4c, fourth panel) and EEJ (third panel) turned strongly eastward, and ended when IMF B_z returned to positive and EEJ(storm) reached its peak; this indicates that there was a strong eastward PPEF during the rapid response. The EEJ data is of 1 h resolution.

[19] Figures 5a and 5b show the rapid F_2 layer drift at Trivandrum during the main phase of the superstorm (Dst = −235 nT) of 12 August 2000. This is a somewhat unusual event. There was a morning counter electrojet (Figure 5b, third panel), which resulted in lower than normal h_mF_2 and higher than normal Nmax until about 1115 LT. Then Nmax (f_oF_2) decreases from about 13.5 MHz to 10.75 MHz at around 1415 LT, which gives a rapid response duration of about 3 h and a f_oF_2 reduction of about 2.75 MHz. The real peak height hmax obtained from true height profiles (not shown) is found to rise from about 475 km to 625km during 1200–1300 LT giving an average real rise velocity of 41 m s^{-1}. The virtual height (h_pF_2) rises from about 500 km to 660 km

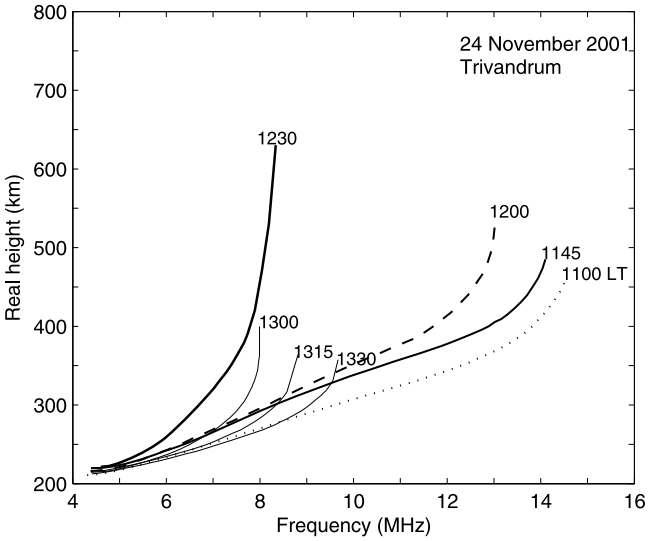

Figure 4b. True height profiles at Trivandrum at selected local times on 24 November 2001.

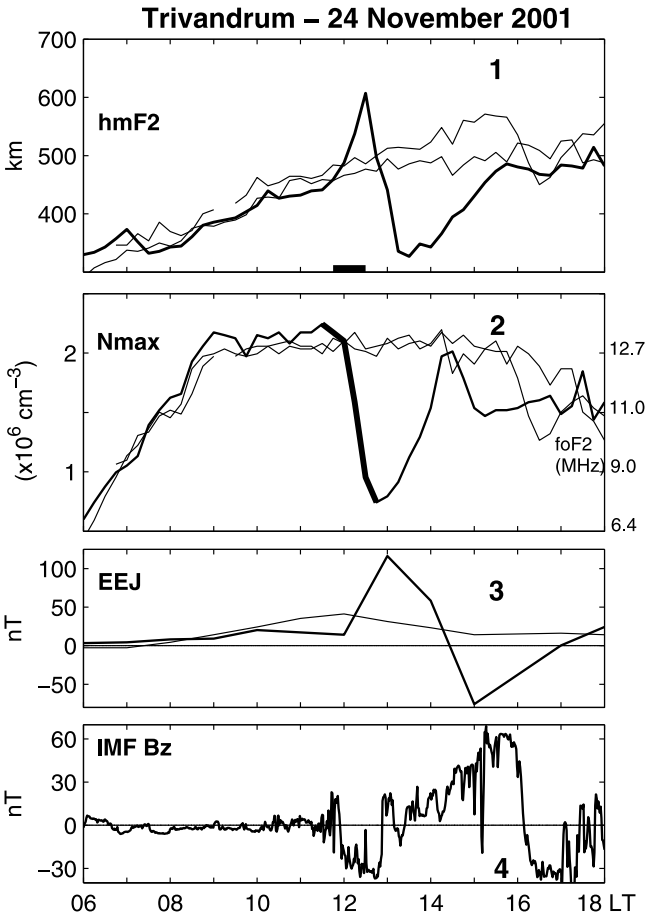

Figure 4c. Variations of h_mF_2 and Nmax (first and second panels) at Trivandrum during 0600–1800 LT on the geomagnetic storm day (24 November 2001, thick curves) compared with those on 3 previous quiet days (thin curves). The small horizontal bar in the first panel represents the duration used for obtaining the virtual rise velocity. The fourth and third panels show the IMF B_z (shifted by 30 min) and equatorial electrojet (thick curve) in the longitude of Trivandrum on the storm day; the thin curve in the third panel is the quiet time electrojet.

during 1200–1300 LT (Figure 5a) giving an average virtual rise velocity of about 45 m s^{-1}. As shown by Figure 5b, the rapid response started when IMF B_z turned from positive to highly negative (up to −25 nT, fourth panel) and when the electrojet turned from westward to eastward (third panel), and ended when the electrojet became weak. This again indicates that the rapid response was produced by an eastward PPEF event. The EEJ data is of 1 h resolution. The two examples at Indian longitude also illustrated that the peak height undergoes rapid rise (and fall) with large Nmax reduction during the daytime main phase of superstorms due to eastward PPEF.

4.3. Australian Longitude

[20] Figure 6a shows part of the repeated occurrence of the rapid F_2 layer drift over the Australian longitude station Vanimo (12.6°S, 141.4°E; 11.8°S) during the main phase of the superstorm (Dst = −373 nT) of 8 November 2004. The

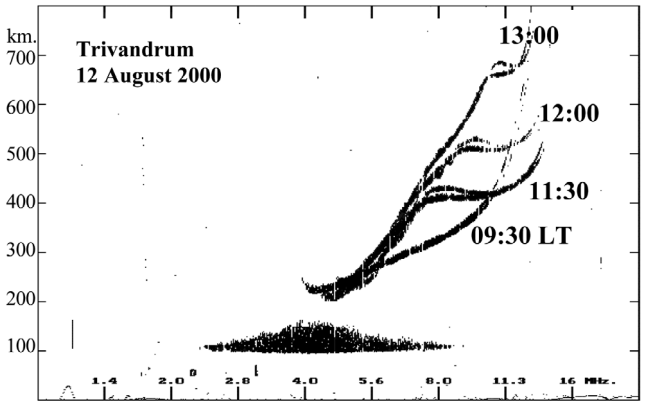

Figure 5a. Four ionograms recorded at the Indian equatorial station Trivandrum (8.5°N, 77°E; 0.5°N) at selected times during the superstorm of 12 August 2000 (Dst = −235 nT) are superposed.

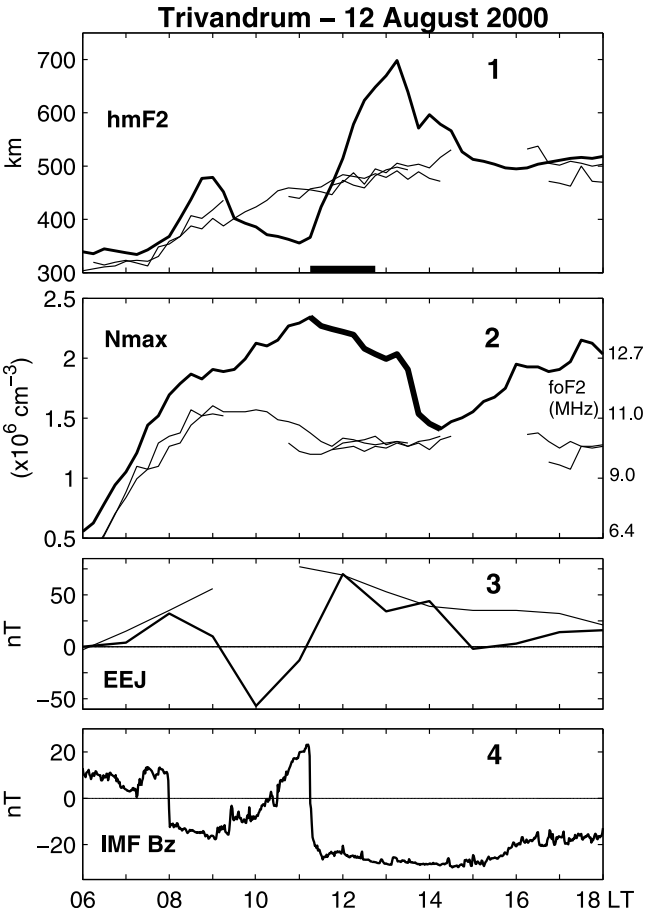

Figure 5b. Variations of h_mF_2 and Nmax (first and second panels) at Trivandrum during 0600–1800 LT on the geomagnetic storm day (12 August 2000, thick curves) compared with those on 3 previous quiet days (thin curves). The small horizontal bar in the first panel represents the duration used for obtaining the virtual rise velocity. The fourth and third panels show the IMF B_z (shifted by 40 min) and equatorial electrojet (thick curve) in the longitude of Trivandrum on the storm day; the thin curve in the third panel is the quiet time electrojet.

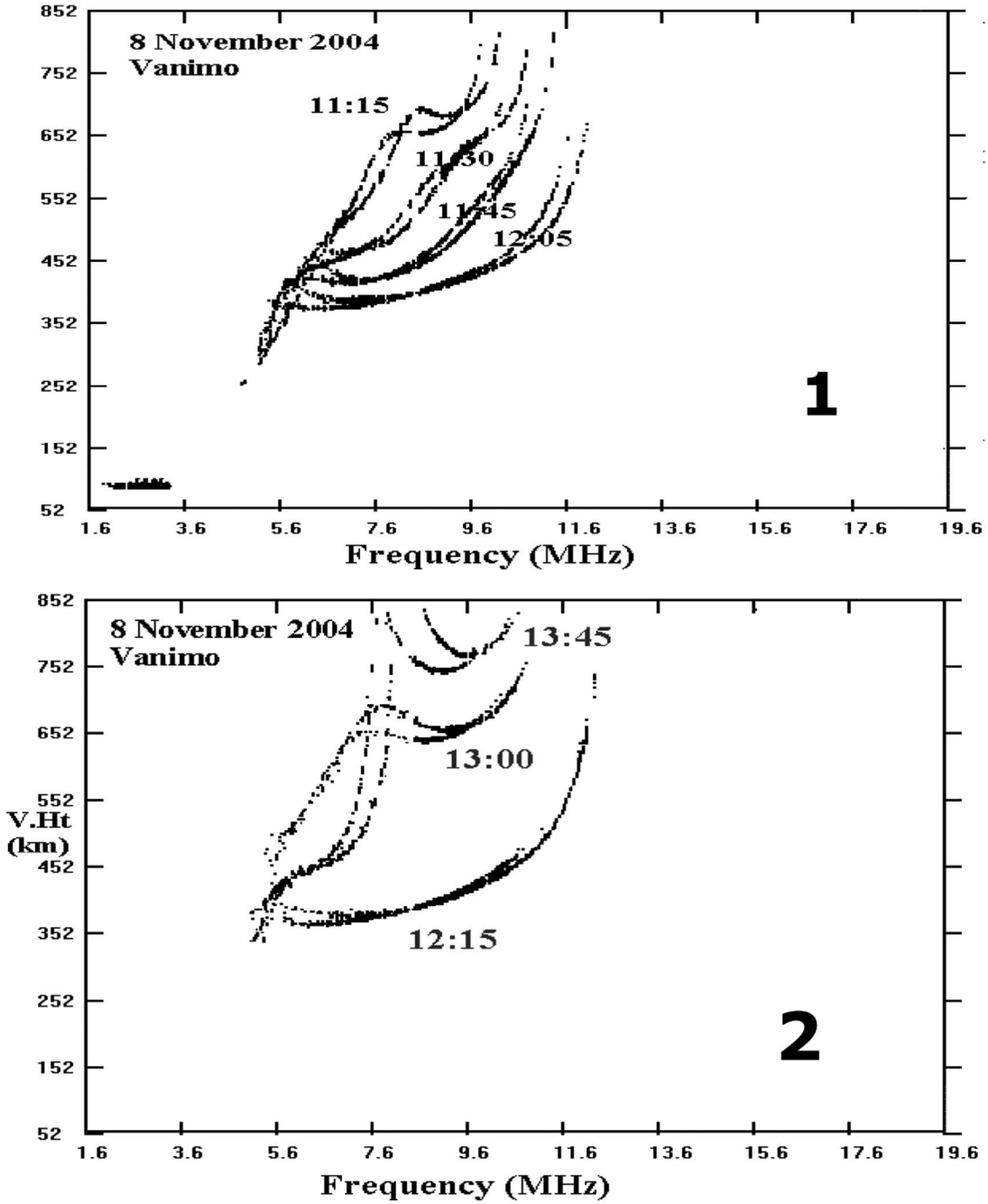

Figure 6a. Four ionograms each recorded at the Australian longitude station Vanimo (12.6°S, 141.4°E; 2.7°S) during 1115–1205 LT (first panel) and 1215–1345 LT (second panel) during the main phase of the superstorm (*Dst* = −373 nT) of 8 November 2004.

observations are not complete because there is a data gap before 1100 LT. As shown by the superposed ionograms at selected times in Figure 6a (first panel), a high-altitude layer (which might have been an F_3 layer drifted to the topside before 1100 LT) drifts downward and merges with the newly formed F_2 layer during 1115–1205 LT; the downward drift, which is unusual during daytime, could be caused by a westward electric field due to prompt penetration and/or disturbance dynamo. By 1200 LT the layer reaches its lowest height (Figure 6b) with f_oF_2 about 11.75 MHz. Then f_oF_2 decreases to about 10.5 MHz by 1345 LT. This gives a rapid response duration of about 1.75 h and a f_oF_2 reduction of about 1.25 MHz. The real height hmax (Figure 6b) rises steadily from around 440 km to 590 km during 1215–1300 LT giving an average real rise velocity of about 56 m s^{-1}. During this period, the virtual height h_pF_2 (Figure 6a, second panel) rises from about 460 km to 660 km, which gives an average virtual rise velocity of about 74 m s^{-1}. The rapid response should be caused by an eastward PPEF event.

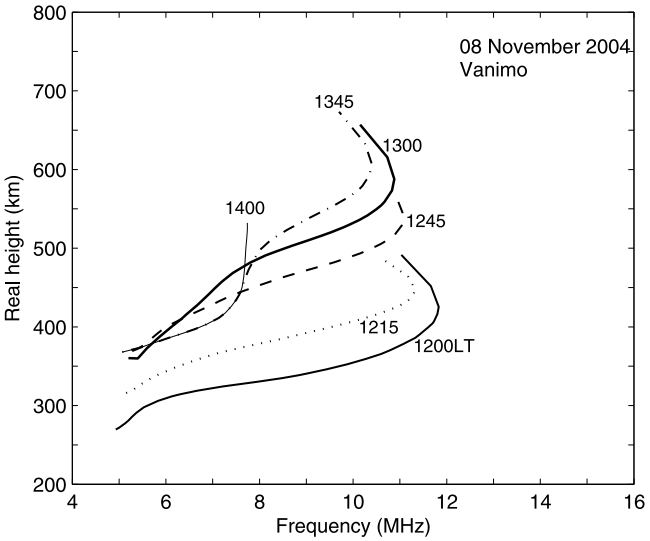

Figure 6b. True height profiles at Vanimo at selected local times on 8 November 2004.

[21] The variations of IMF B_z and EEJ(storm) during the main phase of the storm are shown in Figure 6c, which reveals repeated occurrence of three eastward electrojet (or PPEF) events superposed with a westward electric field. The start and end of the rapid F_2 layer response (Figure 6a, second panel) corresponds to the last eastward PPEF event, and the downward drift of the previous F_2 layer corresponds to the westward electric field event prior to the last eastward PPEF event. The electric field during this storm was studied in detail by *Fejer et al.* [2007] who showed that the three eastward EEJ(storm) events are due to eastward PPEFs. The westward electric field over which the PPEF events are superposed could be due to disturbance dynamo electric field [e.g., *Blanc and Richmond*, 1980; *Abdu et al.*, 2006] and/or penetration from region 2 field-aligned currents [e.g., *Kikuchi et al.*, 2008].

[22] The second example of a rapid F_2 layer response at Australian longitude (Figure 7a) is during the superstorm (Dst = −292 nT) of 6 November 2001. The ionosphere was behaving normally until about 1115 LT. Then f_oF_2 is found to decrease from about 13.5 MHz at 1115 LT to 8 MHz at 1330 LT giving a rapid response duration of about 2.25 h and a large f_oF_2 reduction of about 5.5 MHz (Figure 7a, ionograms up to 1215 LT only are shown). The virtual height h_pF_2 is found to rise steadily from about 670 km to 950 km during 1115–1215 LT (Figure 7a), which gives an average virtual rise velocity of about 78 m s^{-1}. However, the real peak height hmax obtained from true height profiles (not shown) is found to rise steadily during 1130–1215 LT, from about 480 km to 630 km giving an average real rise velocity of about 55 m s^{-1}. This rapid response also started when IMF B_z became highly negative and EEJ(storm) suddenly became strongly eastward (Figure 7b), and ended when EEJ(storm) became weak; this indicates that the rapid response was produced by an eastward PPEF. As mentioned above (section 3), the F_3 layer signatures during the rapid F_2 layer drifts are not considered.

[23] Following the rapid response (Figure 7a, first panel), a topside ledge drifted downward and merged with the newly produced F_2 layer during 1430–1515 LT, and f_oF_2 increased to about 12 MHz (Figure 7a, second panel). This corresponds to the strong westward electric field that followed the eastward PPEF (Figure 7b, first panel). The penetration of the electric field during this event was studied in detail by *Kikuchi et al.* [2008]. The two examples in the Australian longitude also illustrated the daytime rapid rise (and fall) of the F_2 layer with large Nmax reductions due to eastward PPEF. The examples also showed the rare events of strong daytime westward electric fields due to disturbance dynamo and/or prompt penetration from region 2 field-aligned currents.

4.4. Statistics

[24] The statistics of the geomagnetic storms and F_2 layer drift are presented here. As shown by the days of the storms (Figure 8, fourth panel), the storms occur in all seasons and all levels of solar activity though the storms are frequent (10 out of 26) in October–November and at high solar activity (14 in 1998–2002). The intensity of the storms (Dst, first panel) varies from about −150 nT to −420 nT. The maximum negative value of IMF B_z and maximum solar wind velocity of the CMEs that produced the storms are shown in Figure 8, second and third panels. IMF B_z varies from about −10 nT to −80 nT while solar wind velocity ranges from about 500 km s^{-1} to 1850 km s^{-1}. Note that a break symbol is used to fit the large wind velocity (1850 km s^{-1}) on 29 October 2003 [*Skoug et al.*, 2004] within the scale of the other storms.

[25] The blue, red, and green circles in Figure 8 correspond to the storms that have daytime MP in Brazilian, Indian, and Australian longitudes. In each longitude solid circles and circled plus signs represent daytime MPs that

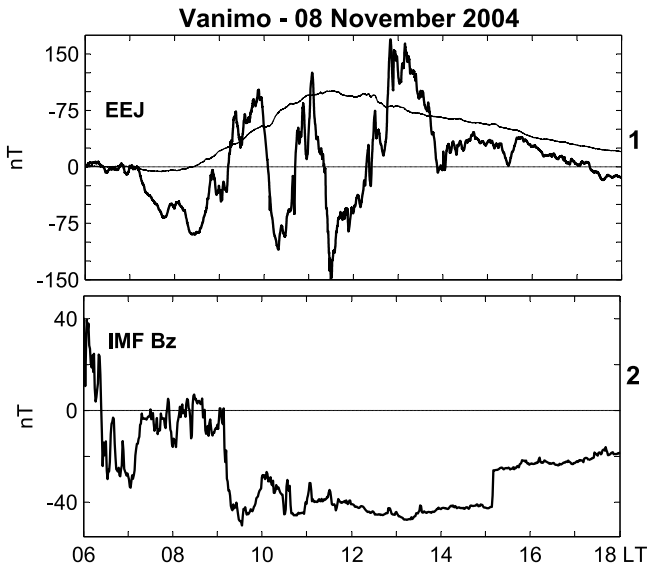

Figure 6c. Variations of IMF B_z (shifted by 35 min, second panel) and equatorial electrojet (first panel, thick curve) during 0600–1800 LT on the geomagnetic storm day (8 November 2004) in the longitude of Vanimo; thin curve (first panel) shows quiet time electrojet.

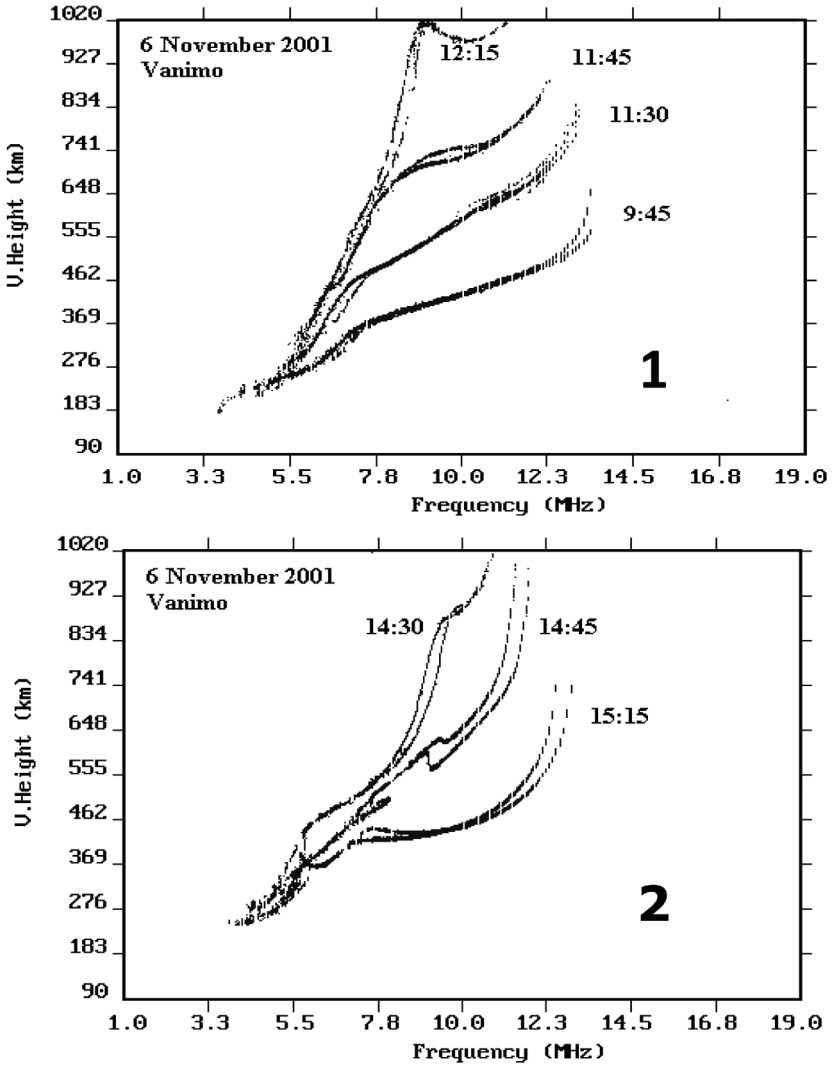

Figure 7a. Ionograms recorded at the Australian longitude station Vanimo (12.6°S, 141.4°E; 2.7°S) during 0945–1215 LT (first panel) and 1430–1515 LT (second panel) during the main phase of the superstorm (*Dst* = −292 nT) of 6 November 2001.

produced rapid (>30 m s^{-1}) and normal (or slow) F_2 layer response, and open circles correspond to nonavailability of ionosonde data. Considering all longitudes together, out of the 22 storms for which ionosonde data are available, 20 storms including all 15 superstorms produced rapid F_2 layer response.

[26] Figure 8 also shows that of the 20 rapid F_2 layer events, 9 are in summer months, 6 are in winter months and 5 are in equinox months; summer months in Indian longitudes are May–August, which are winter months in Brazilian and Australian longitudes. Solar activity wise, the 20 rapid F_2 layer events are distributed as 9 during high solar activity (1998–2002), 8 during medium solar activity (2003–2004) and 3 during low solar activity (2005–2006). As shown by the statistics, the occurrence of rapid F_2 layer response is independent of season and seems to depend on solar activity. However, a greater number of rapid F_2 layer events occur at solar maximum mainly because there are a greater number of storms at solar maximum.

[27] The characteristics of the rapid F_2 layer events are shown in Figure 9. The days of the storms are repeated (fourth panel) and the same color code as in Figure 8 is used for easy reference. The duration of the daytime MP of the storms is shown by the open histograms in the third panel; daytime is taken as 0500–2000 LT to account for possible dawn and dusk events. The solid and crosshatched histograms together within the open histograms (third panel) represent the local time durations of the rapid F_2 layer response (when Nmax undergoes large reductions), with the crosshatched histograms representing the durations used for calculating the average virtual rise velocities. The hatched histograms within the open histograms (third panel) correspond to normal (or slow) F_2 layer response. Cases of no ionosonde data are noted. As shown (third panel), the duration of the 20 rapid F_2 layer events varies from about 1 to 6 h, which seem to agree with the duration of eastward PPEF [e.g., *Huang*, 2008]. There are also three cases when the rapid drift reoccurred, suggesting repeated occurrence of eastward PPEF.

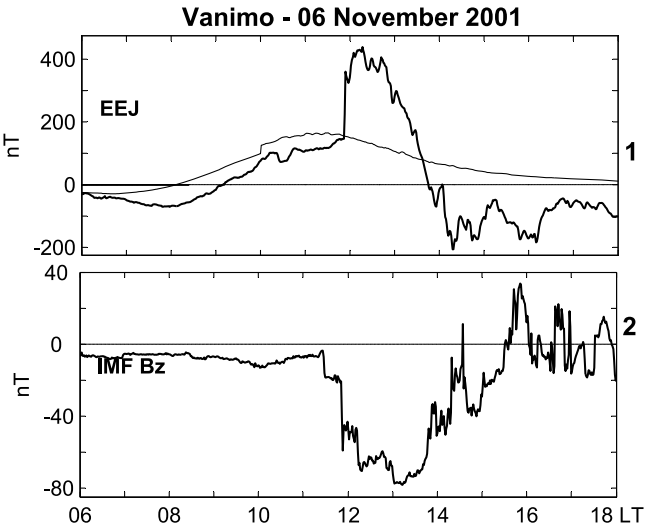

Figure 7b. Variations of IMF B_z (shifted by 60 min, second panel) and equatorial electrojet (first panel, thick curve) during 0600–1800 LT on the geomagnetic storm day (6 November 2001) in the longitude of Vanimo; thin curve (first panel) shows quiet time electrojet.

[28] The statistics of the virtual height (h_pF_2) range (when Nmax decreases) are shown by the solid and crosshatched histograms together in Figure 9 (first panel), with the crosshatched histograms representing range considered for calculating the average virtual rise velocity. As shown, the rapid response starts at around 300–450 km virtual height and extends to the upper limit of the ionosonde range in majority of the cases (≈1200 km for Brazilian, 800 km for Indian, and 1020 km for Australian). The average virtual rise velocity (Figure 10) varies from about 27 m s^{-1} to 80 m s^{-1}. Of the 22 storms 20 produce rapid F_2 layer response with virtual rise velocity >30 m s^{-1}, and the 20 storms include all 15 superstorms. The average real rise velocity (of hmax) is also plotted in Figure 10 for the six events. The virtual and real rise velocities increase almost linearly with the intensity of the storms (*Dst*) except for the large scatter; the linear fit is for the virtual rise velocity. The scatter includes the (1) observed fact of less average rise velocity during MPs with fluctuations than during MPs without fluctuations of nearly same intensity, (2) uncertainty(up to 15 min) in measuring the time duration of the rapid rise, (3) variations of the geophysical conditions (solar activity, season and local time), and (4) possibility of the strongest electric field penetration occurring (at least in some cases) in longitudes in between the three ionosondes. The apparent rise velocity

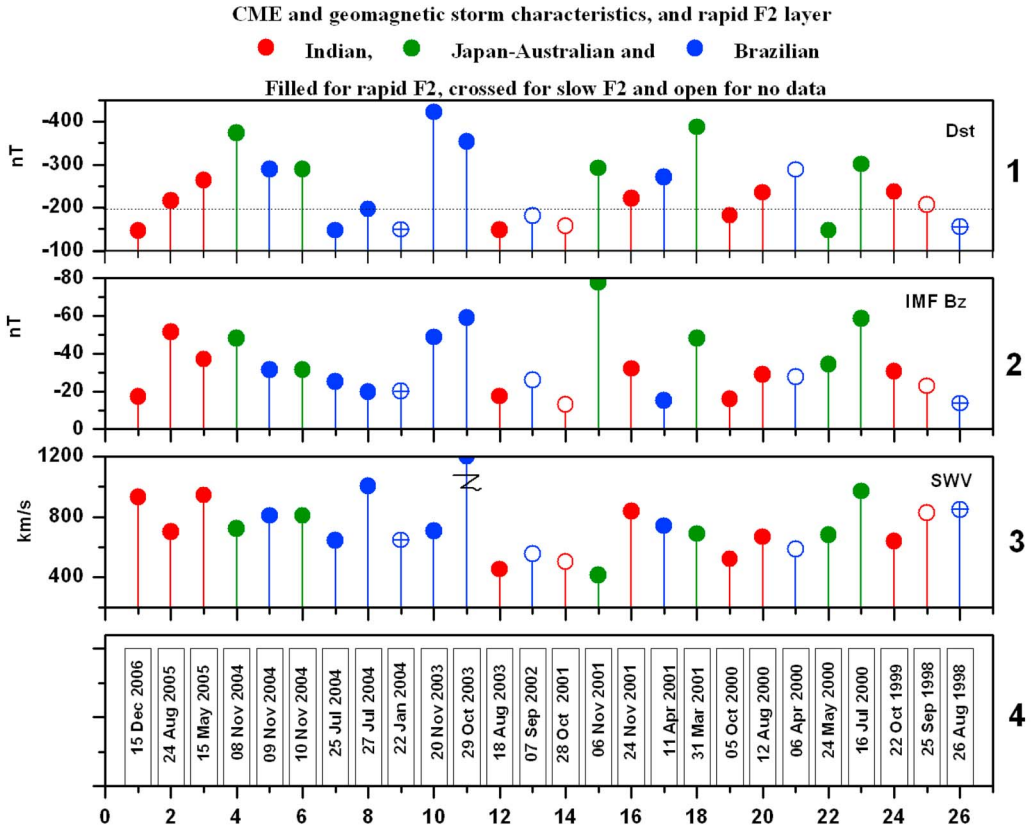

Figure 8. Statistics of the 26 intense storms (*Dst* < −150 nT) and F_2 layer drifts in 1998–2006. The days of the storms (fourth panel), maximum negative *Dst* (first panel), maximum negative IMF B_z (second panel), and maximum solar wind velocity (third panel) are shown. The red, blue, and green circles correspond to Indian, Brazilian, and Australian longitudes; solid circles and circled plus signs represent rapid and normal F_2 layer drifts; and open circles correspond to no data.

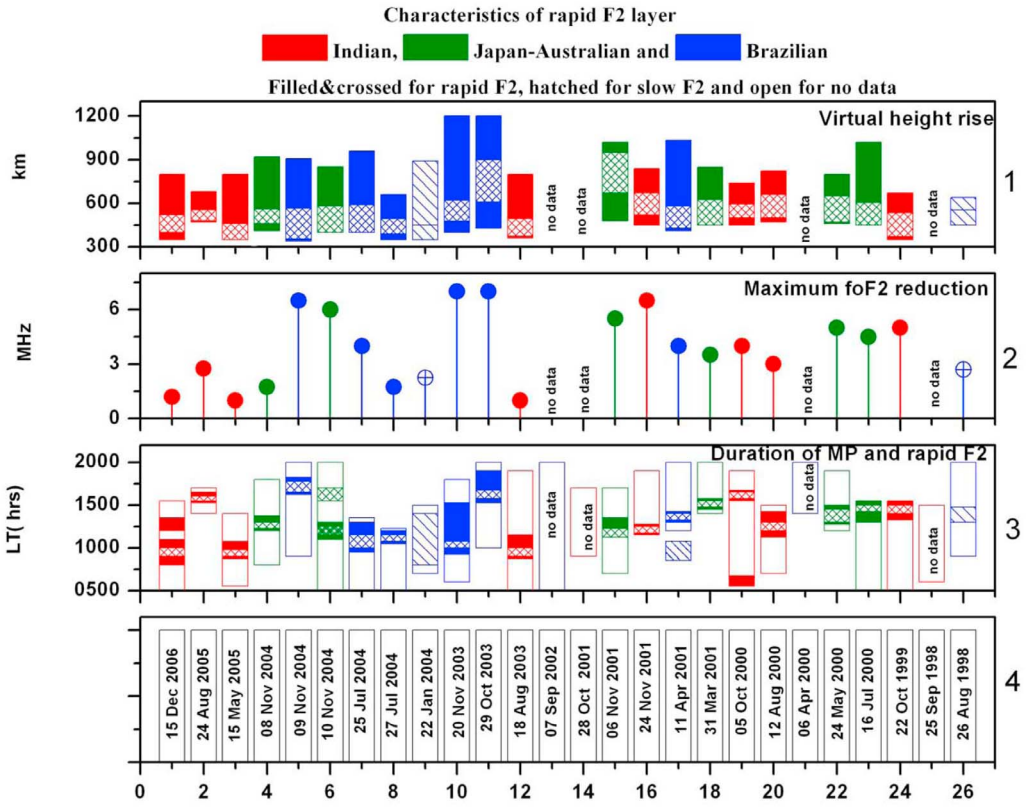

Figure 9. The characteristics of F_2 layer drift: days of storms (fourth panel), duration of daytime main phase (third panel, open histograms), duration of large Nmax reduction (third panel, solid and cross-hatched histograms together), duration used for virtual rise velocity (third panel, crosshatched histograms), duration of normal Nmax reduction (third panel, hatched histograms), virtual height range during large Nmax reduction (first panel, solid and crosshatched histograms together), virtual height range from which average virtual rise velocities are calculated (first panel, crosshatched histograms), and maximum reduction in critical frequency (second panel). Red, blue, and green correspond to Indian, Brazilian, and Australian longitudes; nonavailability of ionosonde data is noted.

goes up to about 80 m s^{-1} (Figure 10) though the real rise velocity is found to be within about 65 m s^{-1}.

[29] Figure 9 (second panel) shows the statistics of the maximum reduction in the critical frequency f_oF_2. The reduction varies from about 1 MHz to 7 MHz. As shown (second panel), all but 2 superstorms have an f_0F_2 reduction >2.5 MHz. It is to be noted that majority of the rapid response events, including the two superstorms events with f_oF_2 reduction <2.5 MHz, are during morning-noon hours (Figure 9, third panel), and a smaller reduction of f_oF_2 during the morning-noon hours of ionization production can be as significant as a larger reduction during afternoon hours. The statistics (Figure 9) therefore seem to verify that the response of the equatorial F_2 layer during the dayside MP of superstorms becomes rapid with large hmax rise (and fall) and large Nmax reduction due to eastward PPEF.

5. Discussion

[30] The digital ionosonde data available at the equatorial locations in Brazilian, Indian and Australian longitudes during 22 intense geomagnetic storms ($Dst < -150$ nT) in 1998–2008 have been analyzed for the characteristics of the daytime F_2 layer response. Of the 22 storms, 20 storms including all 15 superstorms ($Dst < -200$ nT) show rapid rise (>30 m s^{-1}) (and fall) of the F_2 layer peak with large Nmax reduction (>2.5 MHz) during the daytime MP of the storms when IMF B_z remained highly negative and when there was a strong eastward equatorial electrojet. The average rise velocity is also strongly correlated with the intensity of the storms. The statistics therefore suggest that the rapid F_2 layer rise (and fall) with large Nmax reduction happening during the daytime MP of superstorms can invariably be used to monitor the occurrence of eastward PPEF irrespective of season and level of solar activity. The duration of the Nmax reduction may indicate the duration of the PPEF, which can be further checked using the high-resolution EEJ(storm) data.

[31] To further establish a direct link between the rapid F_2 layer response and eastward PPEF, the neutral wind contribution to the rise velocity is to be considered. Though the wind velocities are not available, estimates of their contributions can be made for assumed values. The horizontal winds (and waves) can contribute to the vertical rise velocity of the ionospheric plasma around the equator due to the separation between geomagnetic and geographic equators (or dip angle I) and declination angle (D) through $V_{wind} = U\cos I \sin I$ with $U = U_\theta \cos D + U_\phi \sin D$ where

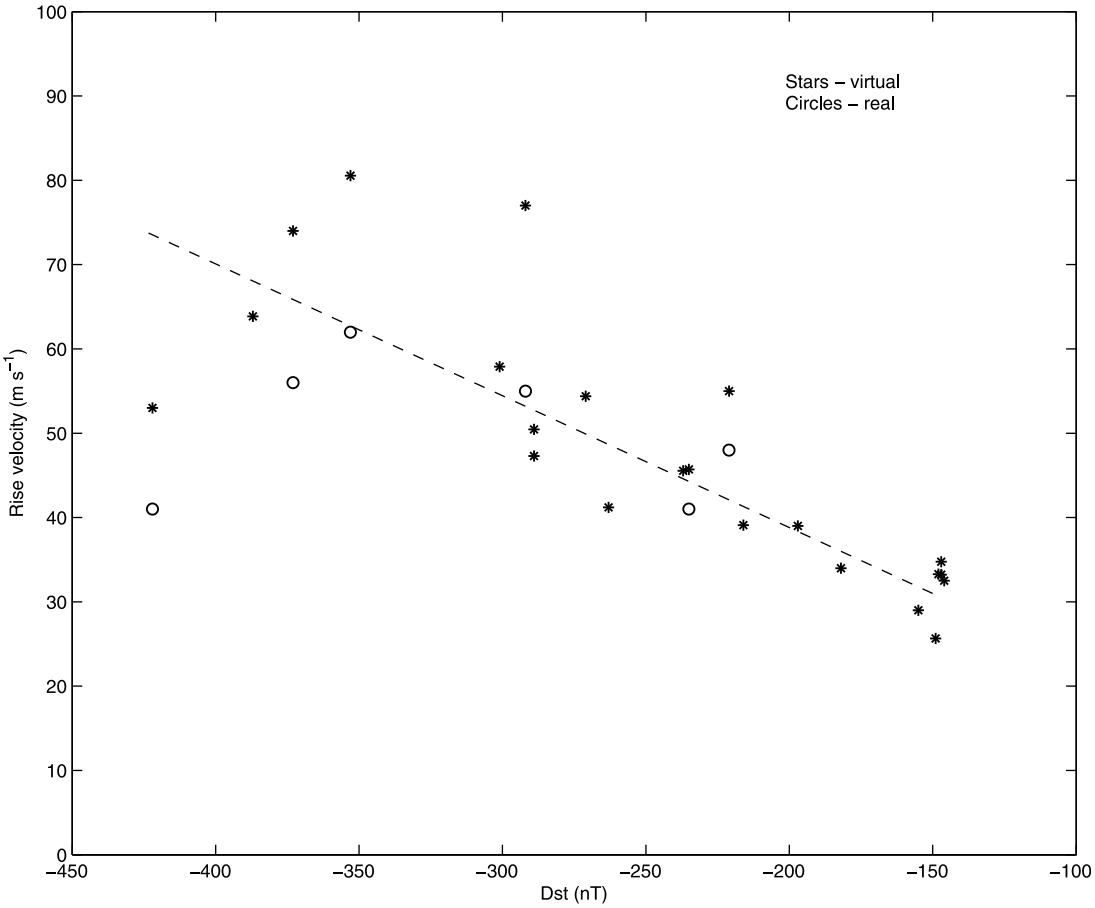

Figure 10. Scatterplot of the average virtual rise velocity (stars) with the intensity of geomagnetic storms (*Dst*), with a linear fit; the open circles show the average real rise velocity.

U_θ (positive southward) and U_ϕ (positive eastward) are the meridional and zonal wind velocities, and D is positive eastward. A meridional wind of 25 m s^{-1} and zonal wind of 100 m s^{-1} can give a vertical plasma rise velocity of about 5.4 m s^{-1} at Vanimo ($I = -22°$, $D = 5.4°$), 3.0 m s^{-1} at Sao Luis ($I = -3°$, $D = -20°$), and 0.25 m s^{-1} at Trivandrum ($I = 0.5°$, $D = 2.25°$). It is also possible for the winds and waves at higher latitudes to contribute indirectly to the observed rapid drifts through E region–F region coupling. The rapid rise velocities obtained from ionosondes can be validated by comparing with those measured by incoherent scatter (IS) radars.

[32] The statistics showed that the rapid F_2 layer response is independent of season and level of solar activity. This is because the main driver of the drift (daytime upward $\mathbf{E} \times \mathbf{B}$) gets strengthened during an eastward PPEF. When the main driver is strong, the possible dependence of the drift on other sources (winds and waves) and hence on season becomes unimportant. The drift becomes independent of solar activity because when the driver is strong enough it can easily drive the F_2 layer peak rapidly upward even at solar maximum when the ionosphere is broad and dense. However, the data (Figures 8 and 9) show frequent occurrence of the rapid drift at equinox (October–November) and at high solar activity, which simply represents the occurrence frequency of the storms.

[33] As mentioned in section 1, the rapid F_2 layer response during the daytime MP of superstorms has been studied earlier mainly for single storms by several investigators. For example, *Paznukhov et al.* [2007] found that the IMF B_z southward turning during the afternoon MP of the superstorm of 9 November 2004 produced a rapid h_mF_2 rise in the low-latitude ionosphere at Jicamarca longitudes. *Fejer et al.* [2007] reported the fastest upward drift velocity (125 m s^{-1}) ever measured by the Jicamarca IS radar during the afternoon MP of this superstorm (9 November 2004). In addition to the rapid F_2 layer drift at Jicamarca on 9 November, such drifts were also observed during daytime at Australian longitude on 8 November and in Indian and Australian longitudes on 10 November during the super double geomagnetic storm of 7–11 November 2004 [*Balan et al.*, 2008]. *Abdu et al.* [2008] reported a real instantaneous upward drift velocity of over 1000 m s^{-1} over the equatorial station Fortaleza in Brazil during the MP of the superstorm of 30 October 2003 using a digital ionosonde and VHF radar. This instantaneous real velocity (1000 m s^{-1}) is much greater than the present average real velocity of 62 s^{-1} and average virtual velocity of 80 m s^{-1}.

[34] As described above, the earlier studies are mainly for single storms, which stressed the rapid h_mF_2 rise during daytime MPs, and not so much the associated Nmax reduction. The present study considered the data from three longitudes for 22 storms in 11 years (1998–2008), and

showed that the rapid rise (and fall) is associated with a large Nmax reduction, the duration of which can indicate the duration of the eastward PPEF; the rise velocity is also shown to increase almost linearly with the intensity of the storms. A physical mechanism for the observations is presented. The statistics also show a few rare events of the rapid downward drifts of the F_2 layer during daytime MPs, which are shown to be due to daytime westward electric fields due to prompt penetration and/or disturbance dynamo. The result is important because IS radars that can directly monitor the PPEF are not available (except the radar at Jicamarca); even high-resolution magnetometers from which PPEF can be inferred through equatorial electrojet are also not available for all longitudes.

6. Conclusions

[35] The analysis of the response of the dayside equatorial F_2 layer to the main phases (MP) of 22 intense geomagnetic storms ($Dst < -150$ nT) in 1998–2008 reveals that there is a period during all MPs when the F_2 layer peak rises (and falls) rapidly with large Nmax reduction; the rise velocity strongly correlates with the intensity of the storms; and the duration of the Nmax reduction agrees with that of the storm time equatorial electrojet. It is therefore suggested that the rapid rise (and fall) of the F_2 layer peak with large Nmax reduction observed by ionosondes during intense storms can be used to detect the occurrence of daytime eastward prompt penetration electric field (PPEF) irrespective of season and level of solar activity. The result is important because radars are not available to monitor the occurrence of PPEF that largely modifies the low-latitude and midlatitude ionosphere, which can cause serious problems in satellite navigation and telecommunication systems.

[36] **Acknowledgments.** N. Balan thanks RISH of Kyoto University for providing a Visiting Professor position. We thank WDC (Kyoto) for the *Dst* data, NICT (Japan) for the Yap and Okinawa magnetometer data, and P. I. D. McComas for the IMF data from ACE.

[37] Robert Lysak thanks the reviewers for their assistance in evaluating this paper.

References

Abdu, M. A. (1997), Major phenomena of the equatorial ionosphere-thermosphere system under disturbed conditions, *J. Atmos. Sol. Terr. Phys.*, *59*, 1505–1519.

Abdu, M. A., J. R. de Souza, J. H. A. Sobral, and I. S. Batista (2006), Magnetic storm associates disturbance dynamo effects over low and equatorial latitude ionosphere, in *Recurrent Magnetic Storms: Corotating Solar Wind Streams*, *Geophys. Monogr. Ser.*, vol. 167, pp. 283–304, doi:10.1029/167GM22, AGU, Washington, D. C.

Abdu, M. A., et al. (2008), Abnormal evening vertical plasma drift and effects on ESF and EIA over Brazil–South Atlantic sector during the 30 October 2003 superstorm, *J. Geophys. Res.*, *113*, A07313, doi:10.1029/2007JA012844.

Alex, S., A. Patil, and R. G. Rastogi (1986), Equatorial counter electrojet—Solution of some dilemma, *Indian J. Radio Space Phys.*, *15*, 114–118.

Anderson, D. N. (1981), Modelling the ambient low latitude *F* region: A review, *J. Atmos. Terr. Phys.*, *43*, 753–762.

Balan, N., and G. J. Bailey (1995), Equatorial plasma fountain and its effects: Possibility of an additional layer, *J. Geophys. Res.*, *100*, 21,421–21,432.

Balan, N., I. S. Batista, M. A. Abdu, J. Macdougall, and G. J. Bailey (1998), Physical mechanism and statistics of occurrence of an additional layer in the equatorial ionosphere, *J. Geophys. Res.*, *103*, 29,169–29,181.

Balan, N., S. V. Thampi, K. Lynn, Y. Otsuka, H. Alleyne, S. Watanabe, M. A. Abdu, and B. G. Fejer (2008), F_3 layer during penetration electric field, *J. Geophys. Res.*, *113*, A00A07, doi:10.1029/2008JA013206.

Balan, N., K. Shiokawa, Y. Otsuka, S. Watanabe, and G. J. Bailey (2009), Super plasma fountain and equatorial ionization anomaly during penetration electric field, *J. Geophys. Res.*, *114*, A03310, doi:10.1029/2008JA013768.

Balan, N., K. Shiokawa, Y. Otsuka, T. Kikuchi, D. Vijaya Lekshmi, K. Kawamura, M. Yamamoto, and G. J. Bailey (2010), A physical mechanism of positive ionospheric storms at low latitudes and midlatitudes, *J. Geophys. Res.*, *115*, A02304, doi:10.1029/2009JA014515.

Batista, I. S., E. de Paula, M. A. Abdu, N. Trivedi, and M. Greenspan (1991), Ionospheric effects of the March 13, 1989, magnetic storm at low and equatorial latitudes, *J. Geophys. Res.*, *96*, 13,943–13,952.

Batista, I. S., M. A. Abdu, J. McDougall, and J. R. Souza (2002), Long term trends in the frequency of occurrence of the *F*3 layer over Fortaleza, *J. Atmos. Sol. Terr. Phys.*, *64*, 1409–1412.

Blanc, M., and A. Richmond (1980), The ionospheric disturbance dynamo, *J. Geophys. Res.*, *85*, 1669–1686.

Fejer, B. G., E. R. de Paula, S. A. Gonzales, and R. F. Woodman (1991), Average vertical and zonal *F* region plasma drifts over Jicamarca, *J. Geophys. Res.*, *96*, 13,901–13,906.

Fejer, B. G., J. W. Jensen, T. Kikuchi, M. A. Abdu, and J. L. Chau (2007), Equatorial ionospheric electric fields during the November 2004 magnetic storm, *J. Geophys. Res.*, *112*, A10304, doi:10.1029/2007JA012376.

Hanson, W. B., and R. J. Moffett (1966), Ionization transport effects in the equatorial *F* region, *J. Geophys. Res.*, *71*, 5559–5572.

Huang, C. S. (2008), Continuous penetration of the interplanetary electric field to the equatorial ionosphere over eight hours during intense geomagnetic storms, *J. Geophys. Res.*, *113*, A11305, doi:10.1029/2008JA013588.

Huang, X., and B. W. Reinisch (1996), Vertical electron density profiles from the Digisonde network, *Adv. Space Res.*, *18*(6), 121–129.

Jin, H., and T. Maruyama (2008), Temporary decrease in daytime *F* region peak electron density due to eastward electric field penetration during magnetic storm, *J. Geophys. Res.*, *113*, A05305, doi:10.1029/2006JA011928.

Kelley, M. C., J. J. Makela, J. L. Chau, and M. J. Nicolls (2003), Penetration of the solar wind electric field into the magnetosphere/ionosphere system, *Geophys. Res. Lett.*, *30*(4), 1158, doi:10.1029/2002GL016321.

Kelley, M. C., M. N. Vlasov, J. C. Foster, and A. J. Coster (2004), A quantitative explanation for the phenomenon known as storm-enhanced density, *Geophys. Res. Lett.*, *31*, L19809, doi:10.1029/2004GL020875.

Kikuchi, T., T. Araki, H. Maeda, and K. Maekawa (1978), Transmission of polar electric fields to the equator, *Nature*, *273*, 650–651.

Kikuchi, T., K. K. Hashimoto, and K. Nozaki (2008), Penetration of magnetospheric electric fields to the equator during a geomagnetic storm, *J. Geophys. Res.*, *113*, A06214, doi:10.1029/2007JA012628.

Lin, C. H., A. D. Richmond, R. A. Heelis, G. J. Bailey, G. Lu, J. Y. Liu, H. C. Yeh, and S. Y. Su (2005), Theoretical study of the low- and mid-latitude ionospheric electron density enhancement during the October 2003 superstorm: Relative importance of the neutral wind and electric field, *J. Geophys. Res.*, *110*, A12312, doi:10.1029/2005JA011304.

Lu, G., L. P. Goncharenko, A. D. Richmond, R. G. Roble, and N. Aponte (2008), A dayside ionospheric positive storm phase driven by neutral winds, *J. Geophys. Res.*, *113*, A08304, doi:10.1029/2007JA012895.

Lynn, K. J. W., T. J. Harris, and M. Sjarifudin (2000), Stratification of the F_2 layer observed in Southeast Asia, *J. Geophys. Res.*, *105*, 27,147–27,156.

Maruyama, T., and M. Nakamura (2007), Conditions for intense ionospheric storms expanding to lower midlatitudes, *J. Geophys. Res.*, *112*, A05310, doi:10.1029/2006JA012226.

Namboothiri, S. P., N. Balan, and P. B. Rao (1989), Vertical plasma drifts in the *F* region at the magnetic equator, *J. Geophys. Res.*, *94*, 12,055–12,060.

Paznukhov, V. V., B. W. Reinisch, P. Song, X. Huang, T. W. Bullett, and O. Veliz (2007), Formation of an F_3 layer in the equatorial ionosphere: A result from strong IMF changes, *J. Atmos. Sol. Terr. Phys.*, *69*, 1292–1304, doi:10.1016/j.jastp.2006.08.019.

Rishbeth, H. (2000), The equatorial *F*-layer: Progress and puzzles, *Ann. Geophys.*, *18*, 730–739.

Sastri, J. H. (1990), Equatorial anomaly in *F* region—A review, *Indian J. Radio Space Phys.*, *19*, 225–240.

Sastri, J., N. Jyoti, V. Somayajulu, H. Chandra, and C. Devasia (2000), Ionospheric storm of early November 1993 in the Indian equatorial region, *J. Geophys. Res.*, *105*, 18,443–18,456.

Skoug, R. M., J. T. Gosling, J. T. Steinberg, D. J. McComas, C. W. Smith, N. F. Ness, Q. Hu, and L. F. Burlaga (2004), Extremely high speed solar wind: 29–30 October 2003, *J. Geophys. Res.*, *109*, A09102, doi:10.1029/2004JA010494.

Sreeja, V., N. Balan, S. Ravindran, T. K. Pant, R. Sridharan, and G. J. Bailey (2009), Additional stratification in the equatorial *F* region at dawn and

dusk during geomagnetic storms: Role of electrodynamics, *J. Geophys. Res.*, *114*, A08309, doi:10.1029/2009JA014373.
Titheridge, J. E. (1985), Ionogram analysis with generalized POLAN, *Rep. UAG-93*, World Data Cent. A for Sol. Terr. Phys., Natl. Oceanic Atmos. Admin., Boulder, Colo.
Vijaya Lekshmi, D., N. Balan, V. K. Vaidyan, H. Alleyne, and G. J. Bailey (2007), Response of the ionosphere to super geomagnetic storms, *Adv. Space Res.*, *41*(4), 548–555, doi:/10.1016/j.asr.2007.08.029.

M. A. Abdu and I. S. Batista, INPE, Av. dos Astronautas 1758, Sao Jose dos Campos 12201-970, Brazil.
S. Alex, Indian Institute of Geomagnetism, Plot 5, Sector 18, Navi Mumbai 410218, India.
N. Balan, Control and Systems Engineering, University of Sheffield, Sheffield S1 3JD, UK. (b.nanan@sheffield.ac.uk)
T. Kikuchi, Y. Otsuka, and K. Shokawa, STE-Lab, Nagoya University, Nagoya 464-8601, Japan.
K. J. W. Lynn, Ionospheric Systems Research, 38 Goodchap St., Noosaville, Qld 4566 Australia.
S. Ravindran and V. Sreeja, Space Physics Laboratory, Vikram Sarabhai Space Centre, Thumba, Trivandrum 695022, India.
M. Yamamoto, RISH, Kyoto University, Kyoto 611-0011, Japan.